Supporting Information

Structure of human ADP-ribosyl-acceptor hydrolase 3 bound to ADP-ribose reveals a conformational switch that enables specific substrate recognition

Yasin Pourfarjam[1,†], Jessica Ventura[1,†], Igor Kurinov[2], Ahra Cho[1], Joel Moss[3], and In-Kwon Kim[1,*]

From the [1] Department of Chemistry, University of Cincinnati, 301 Clifton Ct, Cincinnati, Oh 45221, USA; [2] Cornell University, Department of Chemistry and Chemical Biology, NE-CAT APS, Building 436E, 9700 S. Cass Ave., Argonne, IL 60439; [3] Pulmonary Branch, NHLBI, National Institutes of Health, Bethesda, Maryland 20892

Running title: *Structure of human ARH3 bound to ADP-ribose and Mg^{2+}*

[†] These authors contributed equally to this work.
* To whom correspondence should be addressed: In-Kwon Kim, Department of Chemistry, University of Cincinnati, 301 Clifton Ct, Cincinnati, Oh 45221, USA; E-mail: in-kwon.kim@uc.edu; Tel.: (513) 556-1909; Fax.: (513) 556-9239.

Supporting information contents:

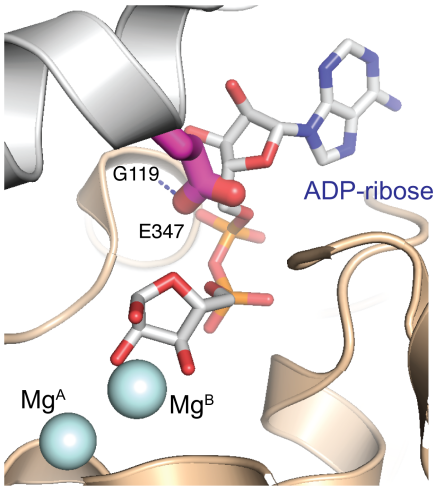

Figure S1. Crystal-packing interactions in apo-ARH3$^{\Delta N16}$ crystals (PDB ID: 2foz) interfere with ADP–ribose (ADPR) binding. The structure of the ARH3^{FL}:ADPR:Mg^{2+} complex, determined in this study, was superimposed onto that of apo-ARH3$^{\Delta N16}$ and ADPR is shown with structures of apo-ARH3$^{\Delta N16}$ (wheat) and its symmetry-related molecule (grey). Glu347 from one ARH3 unit points towards the ADPR-binding cleft of the other ARH3 unit in apo-ARH3$^{\Delta N16}$ crystals, forming a hydrogen bond with the main chain nitrogen of Gly119. This crystal-packing arrangement interferes with ADPR binding. The numbering of amino acid residues here deviates by 16 from that used for the apo-ARH3$^{\Delta N16}$ structure[1].

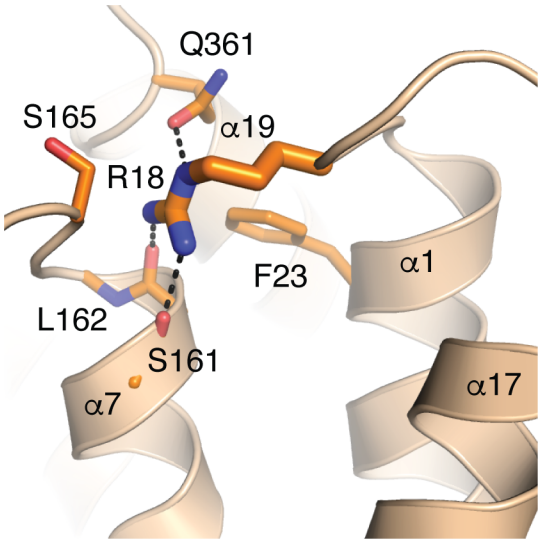

Figure S2. Arg18 in the N-terminal extension stabilizes ARH3 folding. Arg18, which was previously replaced by alanine in the apo-ARH3$^{\Delta N16}$ structure[1], participates in ARH3 folding. Arg18 forms H-bonds with main chain carbonyls of Ser161 and Leu162 in α7, stabilizing the end of α7 by providing helix-capping interactions. Arg18 further stabilizes ARH3 folding by making a hydrogen bond with the side chain carbonyl of Gln361 in α19 and a van der Waals contact with the side chain of Phe23 of α1.

a

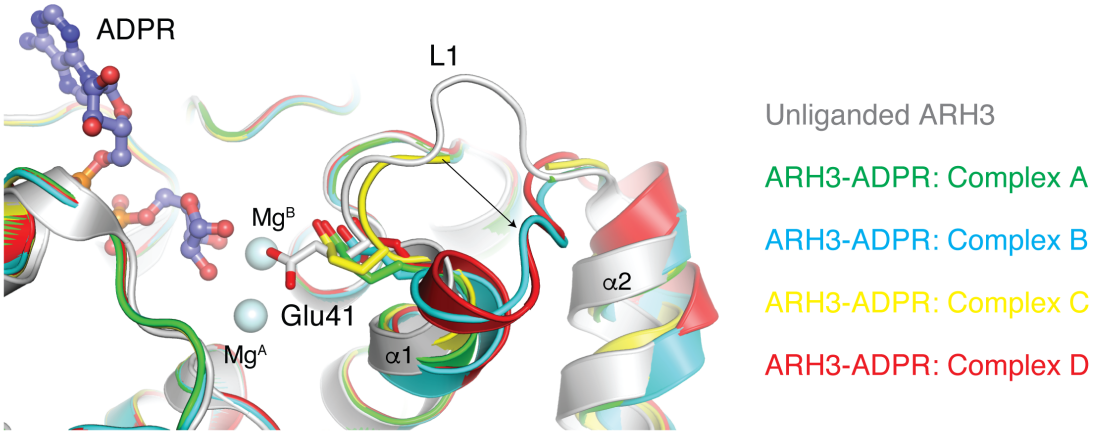

b

	apo-ARH3$^{\Delta N16}$	Complex A	Complex B	Complex C	Complex D
apo-ARH3$^{\Delta N16}$		0.9 Å	1.3 Å	0.9 Å	1.4 Å
Complex A	0.9 Å		0.5 Å	0.5 Å	0.6 Å
Complex B	1.3 Å	0.5 Å		0.8 Å	0.4 Å
Complex C	0.9 Å	0.5 Å	0.8 Å		0.8 Å
Complex D	1.4 Å	0.6 Å	0.4 Å	0.8 Å	

rmsd between ARH3 structures.

Figure S3. Structural comparison of apo-ARH3$^{\Delta N16}$ and four ARH3^{FL}:ADPR:Mg^{2+} complexes in the asymmetric unit of the ARH3^{FL}:ADPR:Mg^{2+} crystals. **a** Structural overlay of apo- and ADPR-bound forms of ARH3. With respect to the apo-ARH3$^{\Delta N16}$ structure, complexes B and D show a straightened α1 conformation with a large displacement of L1, whereas complexes A and C exhibit an intermediate state between apo-ARH3$^{\Delta N16}$ and complexes D. In all four ARH3-ADPR complexes, Glu41 in the Glu_{41}-flap moved away from Mg^B, allowing PAR substrate to enter the binuclear metal center. **b** Rmsd difference between apo- and ADPR-bound forms of ARH3 structures. The pairwise rmsd values were calculated using Dali server[2]. The complex D shows the largest conformational transition upon ADPR binding (in panel **a**) with largest rmsd, in comparison to apo-ARH3$^{\Delta N16}$.

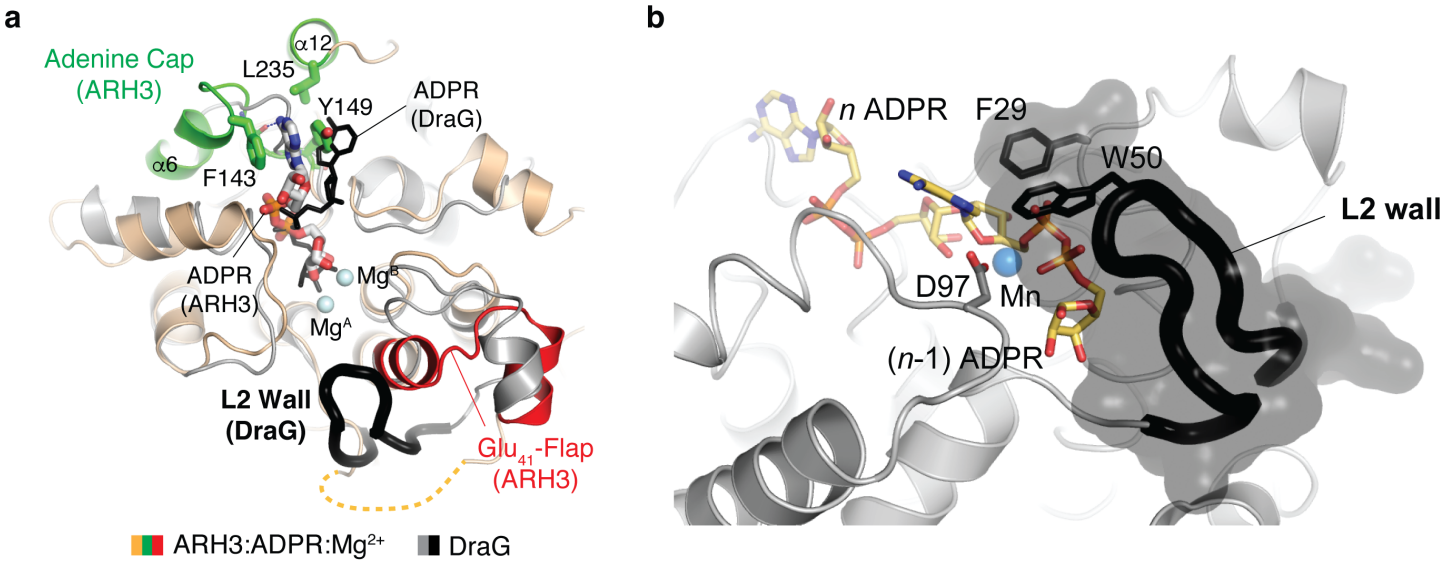

Figure S4. The L2 wall of DraG limits a conformational switch of α1 and L1 (corresponding to the Glu^{41}-flap of ARH3), blocking the access of (*n*-1) ADPR to the active site. **a** Structural superposition of ADPR-bound forms of ARH3 (wheat) and DraG (gray) reveals a distinctive ADPR-binding mode in ARH3. The adenine cap of ARH3 (green) grasps the adenine ring and is essential for ARH3 activities. Hydrogen bonds contributed by the main chain atoms of the adenine cap to N6 and N7 of the adenine ring impart specificity. In contrast to the flexible Glu_{41}-flap of ARH3 (red), the L2 wall in DraG (black) caps α1 and blocks its conformational change. **b** Structural superposition of the ARH3:di-ADPR:Mg^{2+} complex model and DraG reveals that the L2 wall interferes with (*n*-1) ADPR binding to DraG. Trp50 and Phe29 of DraG form an edge-stacking π-π interaction, stabilizing the restrictive conformation of the L2 wall. The corresponding L2 is disordered in ARH3, allowing PAR substrate to access the binuclear metal center. This structural arrangement of L2 in DraG therefore prevents binding and hydrolysis of PAR.

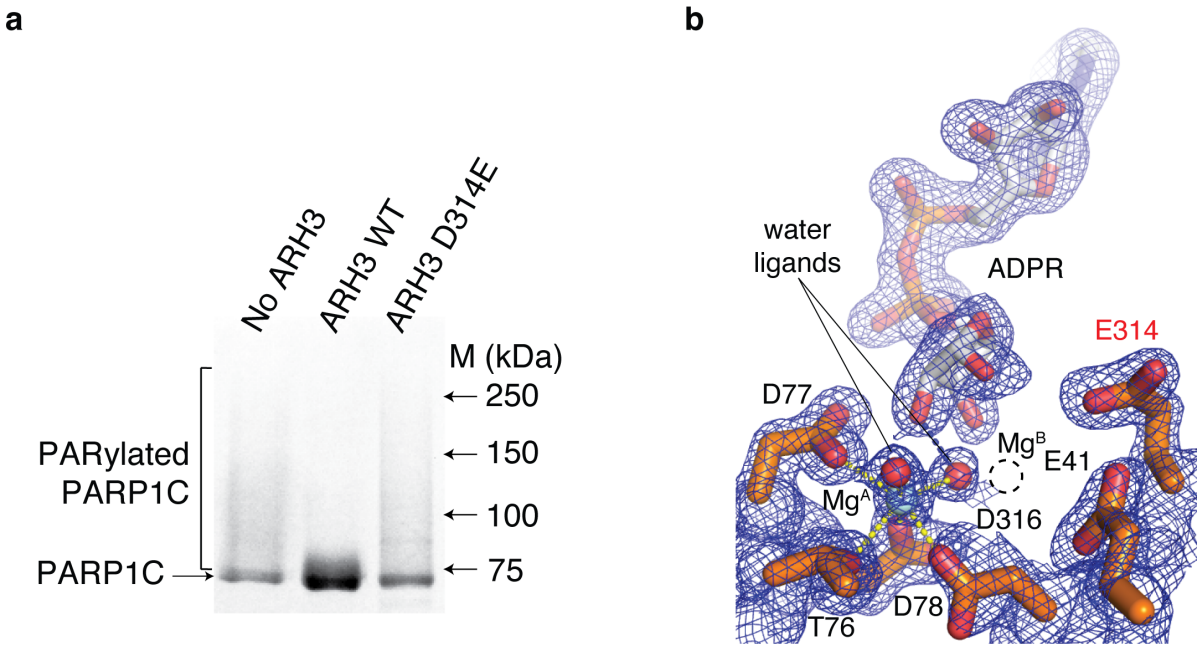

Figure S5. ADP-ribosyl-acceptor hydrolase activity and structure of the ARH3^{D314E}:ADPR:Mg^{2+} complex. **a** The ARH3-D314E mutant is catalytically inactive. ARH3-mediated PAR hydrolysis of the wild-type (WT) and the D314E mutant was measured using a gel-based assay. **b** A $2F_o - F_c$ electron density for the active site of the ARH3-D314E mutant is shown (contoured at 1.0 σ, blue). A position for the missing Mg^B in the ARH3-D314E mutant is shown with a dotted circle. The orientation of this figure is identical to that of Fig. 5.

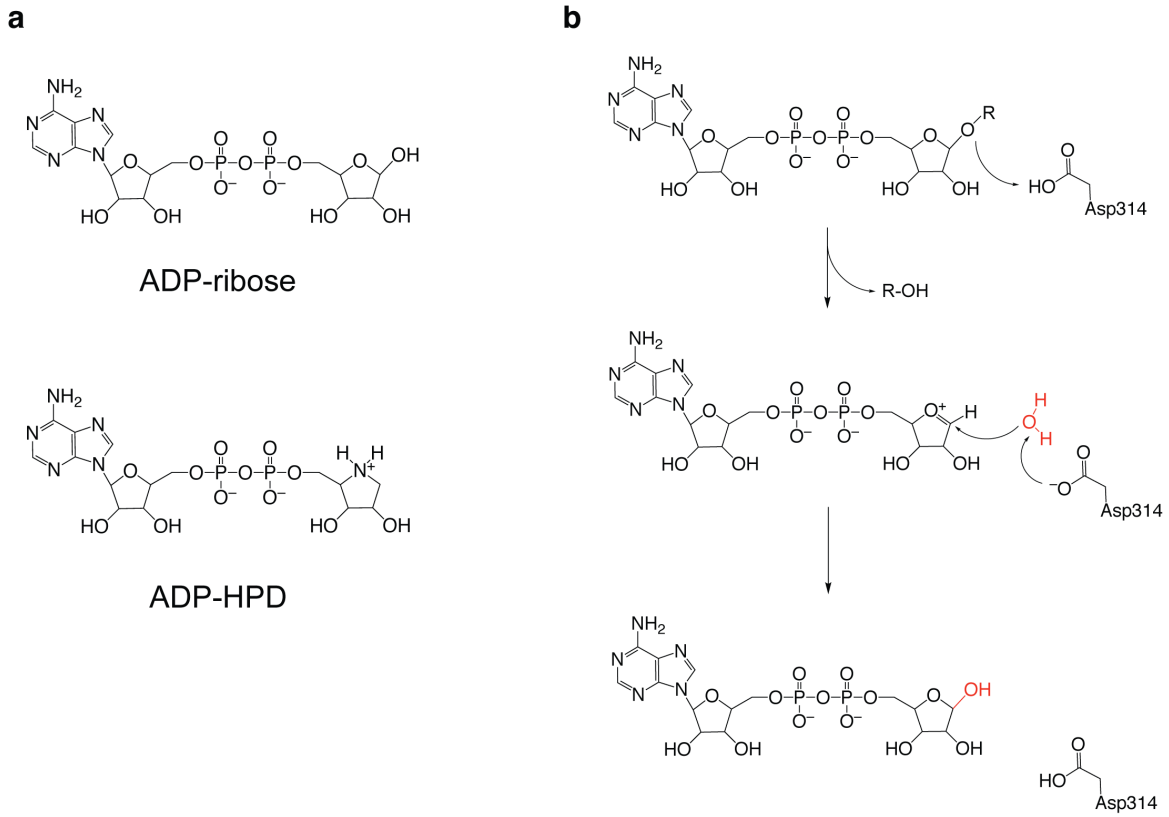

Figure S6. A proposed catalytic role of Asp314. **a** Structures of ADP-ribose and ADP-HPD, an analog of the oxocarbenium ion intermediate of ADP-ribose. **b** A catalytic role of Asp314. Asp314 is located proximal to the 1″-*O*-linkage in substrates. Asp314 might protonate the leaving group (general acid), forming an oxocarbenium ion intermediate, and then activate the water (general base) for back-side attack. The W1 ligand of Mg^{B} (Fig. 3b) can serve as the nucleophile attacking the anomeric C1″ of the ribose″. This is consistent with the observed O^{18} incorporation during hydrolysis of *O*-acetyl-ADP-ribose.

Table S1. Crystallographic data statistics.

	hARH3^{WT}-ADPR complex	hARH3^{D314E}-ADPR complex
Data collection		
Space group	*P*1	*P*1
Cell dimensions		
a, *b*, *c* (Å)	44.9, 72.3, 115.9	44.9, 72.2, 115.9
α, β, γ (°)	83.0, 85.7, 72.0	83.0, 85.7, 72.4
Wavelength (Å)	0.97	0.97
Resolution (Å)	30 – 1.7	30 – 1.6
R_{sym} (%)	6.9 (48.9)	4.5 (43.2)
$I / \sigma I$	21.9 (2.9)	17.6 (3.0)
Completeness (%)	96.6 (98.2)	95.7 (91.3)
Redundancy	3.0 (2.7)	3.9 (3.8)
Refinement		
Resolution (Å)	30 – 1.7	30 – 1.6
No. reflections	146,248	173,752
R_{work} / R_{free}	18.4 / 21.8	16.7 / 19.9
No. atoms		
Protein	10,145	10,197
Ligand/ion	152	148
Water	935	824
B-factors		
Protein	22.1	26.9
Ligand/ion	26.8	31.0
Water	30.2	33.5
R.m.s deviations		
Bond lengths (Å)	0.011	0.007
Bond angles (°)	0.954	0.934

*Values in parentheses are for highest-resolution shell.

Each dataset was collected from a single crystal.

SUPPLEMENTARY REFERENCES

1. Mueller-Dieckmann, C. et al. The structure of human ADP-ribosylhydrolase 3 (ARH3) provides insights into the reversibility of protein ADP-ribosylation. *Proc Natl Acad Sci U S A* **103**, 15026-31 (2006).
2. Holm, L. & Laakso, L.M. Dali server update. *Nucleic Acids Res* **44**, W351-5 (2016).